ORIGINAL RESEARCH ARTICLE

# Solvothermal Synthesis and Growth of Covalent Organic Framework Electrochromic Film with Triphenylamine Active Unit

Shanxin Xiong[1,2] · Yukun Zhang[1] · Wei Zhang[1] · Nana Yang[1] · Fengyan Lv[1] · Jingru Guo[1] · Xin Cui[1] · Ke Fang[1] · Min Chen[1] · Chenxu Wang[1] · Chunxia Hua[1] · Runlan Zhang[1] · Jia Chu[1] · Jianwei Xu[3]

## Abstract

Covalent organic frameworks (COFs) with reversible redox units and a conjugated molecular skeleton possess novel photoelectrochemical properties. In this work, tris(4-aminophenyl)amine and 4,4-biphenyldiformaldehyde were chosen to synthesize TABP-COF electrochromic film with triphenylamine (TPA) active unit by a solvothermal method in a Teflon-lined reactor. The growth process and reaction time optimization of the TABP-COF were studied. TABP-COF shows a self-assembly growth process from an array of nanosheets to nanospheres. Owing to the redox characteristics of TPA, the TABP-COF film exhibits reversible electrochromic behavior. With a solvothermal reaction time of 72 h, the TABP-COF-3 film exhibits the best electrochromic properties, including contrast of 0.483 and response time of 7.3 s/13.6 s. Considering the abundance of redox-active units that can be chosen, COF materials with different redox units and color changes can be designed for a variety of applications in the field of electrochromic materials.

## Introduction

In the twenty-first century, the development of energy-saving and environmentally friendly materials has become particularly important in addressing the depletion of non-renewable resources.[1] Electrochromism can be defined as the reversible change in a material's color and optical features when different voltages are applied to it.[2–4] At present, problems of single color change and long response time limit the application of inorganic electrochromic materials.[5,6] Organic electrochromic materials, represented by conductive polymers, show better color-control ability and application prospects.[7,8]

✉ Shanxin Xiong
   xiongsx@xust.edu.cn

1   College of Chemistry and Chemical Engineering, Xi'an University of Science and Technology, Xi'an 710054, People's Republic of China

2   Key Laboratory of Coal Resources Exploration and Comprehensive Utilization, Ministry of Land and Resources, Xi'an 710021, People's Republic of China

3   Institute of Sustainability for Chemicals, Energy and Environment, Singapore 138634, Singapore

However, issues of poor stability in conductive polymers have not been solved.

Covalent organic frameworks (COFs) are a special class of conductive polymers in which the molecular structure is formed by light element cross-linking.[9,10] Two-dimensional (2D) COFs have a $\pi$–$\pi$ conjugated molecules structure in the 2D plane and strong interlayer electron transfer, which can provide good electrochemical properties for these materials.[11,12] COFs have been widely used in the field of catalyst carriers,[13,14] storage and separation of gas,[15] and as photoelectric materials[16,17] because of their adjustable pore size and molecular constitution.[18] Xu et al.[19] prepared CNT@TFA-COF-3 by introducing carboxylated multi-walled carbon nanotubes (MWCNT) into triazinyl COF (TFA-COF) using a one-pot method. CNT@TFA-COF-3 showed good crystallization, a large specific surface area (1034 m$^2$/g), high specific capacitance (338 F/g), and excellent cyclic stability. It can be found that the peculiarities of COFs are closely correlated with the functional groups of the constitutional unit and skeleton structure. If units with electrochromic activity are incorporated into a COF structure, electrochromic COF materials can be obtained. Xiong et al.[20,21] and Hao et al.[22,23] have demonstrated the electrochromic properties of COF.

In recent research, triphenylamine (TPA) and its derivatives have been applied in the field of electrochromism because the strong electron giving ability of TPA can bind to other electron acceptors to form a wide electron delocalization, and TPA has the characteristics of reversible redox behavior by electrochemical methods.[24–26] Niu et al.[27] designed and synthesized a polyamide (PA) containing TPA-based pyrrole nuclei, which exhibited reversible electrochemical oxidation behavior with film color transition from yellow to blue. In particular, the PA film had high coloring efficiency and cycle stability. Thus, TPA can be used as a monomer to provide redox properties in structural units of COF, which can contribute to the generation of electrochromic behavior of COF films. In our previous work, the electrochromic properties of COF materials combined with TPA and trialdehydes were studied.[21,28] TPA-based COF electrochromic films with different structures are worth studying in depth.

In this work, TABP-COF is designed and synthesized by a solvothermal method using tris(4-aminophenyl) amine (TAPA) and 4,4-biphenyldiformaldehyde (BPDA) as triamine and dialdehyde units, respectively. The growth process of TABP-COF is investigated. The structural characteristics and electrochromic properties of the TABP-COF film are tested, and the relationship between the molecular structure and electrochromic properties is discussed.

## Experimental

### Materials

Tris(4-aminophenyl)amine (TAPA) was purchased from Kaiyulin Pharmaceutical Technology Co., Ltd. (China). 4,4-Biphenyldiformaldehyde (BPDA), ethylene glycol, propylene carbonate (PC), LiClO$_4$, and N,N-dimethyl formamide (DMF) were purchased from Aladdin Co., Ltd (China).

o-Dichlorobenzene and 1,6-hexamethylene diamine were purchased from Shanghai Macklin Biochemical Technology Co., Ltd. (China). Indium tin oxide (ITO) glass was purchased from Shenzhen Huanan Xiangcheng Technology Co., Ltd. (China). All chemicals were used directly without further purification.

### Amination Treatment of ITO Glass

ITO glass, cut to 1 cm × 5 cm, was ultrasonically cleaned with acetone, ethanol, and deionized water successively for 20 min. The ITO glass was then put into a Teflon reactor with 1,6-hexamethylene diamine (2 g) and ethylene glycol (20 mL) and reacted at 200°C for 3 h. Finally, the treated ITO glass was dried after an ethanol rinse.

The contact angles of the ITO glass and ITO glass after amination treatment were measured (Fig. 1). It can be seen that the contact angle of the ITO glass after amination treatment decreased from 52.0° to 43.5°. This indicates that the hydrophilicity of the ITO glass surface increased after the amination treatment, which provides favorable conditions for the subsequent hydrothermal reaction film formation. In addition, the adhesion of the film can be enhanced by the amino functional group on the ITO glass.

### Synthesis of TABP-COF Films

First, TAPA (0.014 g, 0.05 mmol) and BPDA (0.015 g, 0.075 mmol) were dissolved in mixtures of o-dichlorobenzene (6 mL) and anhydrous ethanol (1 mL), respectively. ITO glass was put into a Teflon lined reactor with the TAPA solution. The reactor was pre-heated for 10 min at 90°C. BPDA solution was then added to the reactor with a dropping speed of 1 mL/min. The lid of the reactor was closed quickly followed by reaction at 90°C for a period of time. After cooling, the ITO glass, which had a yellow film, was ultrasonically cleaned with anhydrous ethanol. The powder residue in the reactor was centrifuged and washed with DMF
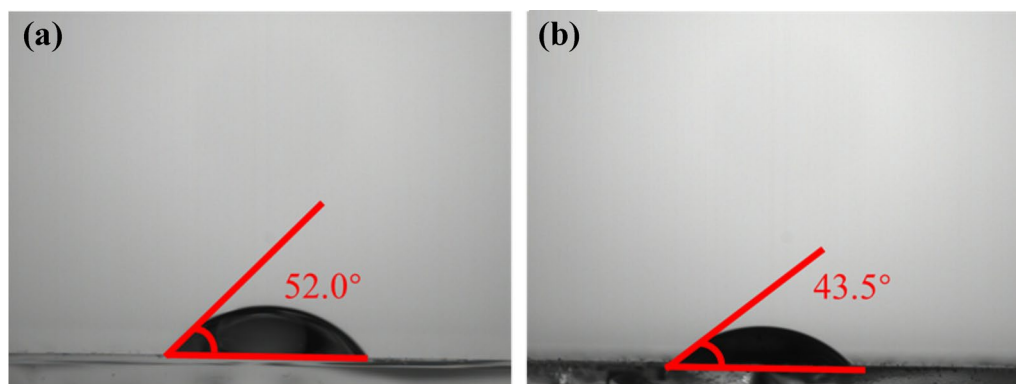


**Fig. 1** Surface contact angle of ITO glass (a) and after amination treatment (b).

and anhydrous ethanol, then dried overnight in a vacuum oven at 60°C. The TABP-COF materials with reaction times of 24 h, 48 h, and 72 h were denoted as TABP-COF-1, TABP-COF-2, and TABP-COF-3, respectively. Figure 2 exhibits the synthetic process and molecular structure of TABP-COF.

## Preparation of Electrolyte Solution

The electrolyte was a 0.1 mol/L $LiClO_4$ solution, prepared by ultrasound-assisted mixing of $LiClO_4$ (0.512 g) and PC (50 mL) for 15 min.

## Characterization

Scanning electron microscopy (SEM, Phenom Pro, Thermo Fisher Scientific) was used for testing the surface morphology of the TABP-COF. The Fourier transform infrared (FTIR) spectra of COF powders were acquired on a Nicolet 60XR FTIR spectrometer using the KBr pellet method. The crystal structure of the COF powders was measured using a Bruker D8 Advance diffractometer. The Raman spectra of the samples were tested using an inVia Reflex laser microRaman spectrometer with an incident wavelength of 785 nm. The thermal stability of the COF materials was determined by a NETZSCH STA 449 F3 thermogravimetric analyzer (TGA) under $N_2$ conditions at a heating rate of 10°C/min for a test range of 30–800°C. Electrochemical tests, including cyclic voltammetry (CV) tests and electrochemical impedance spectroscopy (EIS), of the electrochromic films were conducted using a CHI660E electrochemical workstation (Shanghai Chenhua Instrument Co., Ltd.). The electrochemical tests were carried out with a three-electrode system in 0.1 M $LiClO_4$/PC electrolyte solution with a potential range from −1.5 V to 1.5 V. The ITO conductive glass with TABP-COF film acted as the working electrode. The counter and reference electrodes were Pt plate (99.99%) and Ag/AgCl (3 M KCl), respectively. The ultraviolet–visible (UV–Vis) spectra and kinetic curves of the samples were measured by an electrochemical workstation (Autolab PGSTAT101) coupled with a UV–Vis spectrometer (Shimadzu UV-2550). The test voltages of the UV–Vis spectral curves of the film were 0 V, 1.8 V, and −3 V, respectively, with a wavelength range of 400–800 nm in 0.1 M $LiClO_4$/PC electrolyte solution. The square-wave potentials of the kinetics test were −3.0 V and +1.8 V at a reference wavelength of 550 nm. The contact angle test was conducted using a JC2000DM contact angle measuring instrument (Shanghai Zhongchen Company).
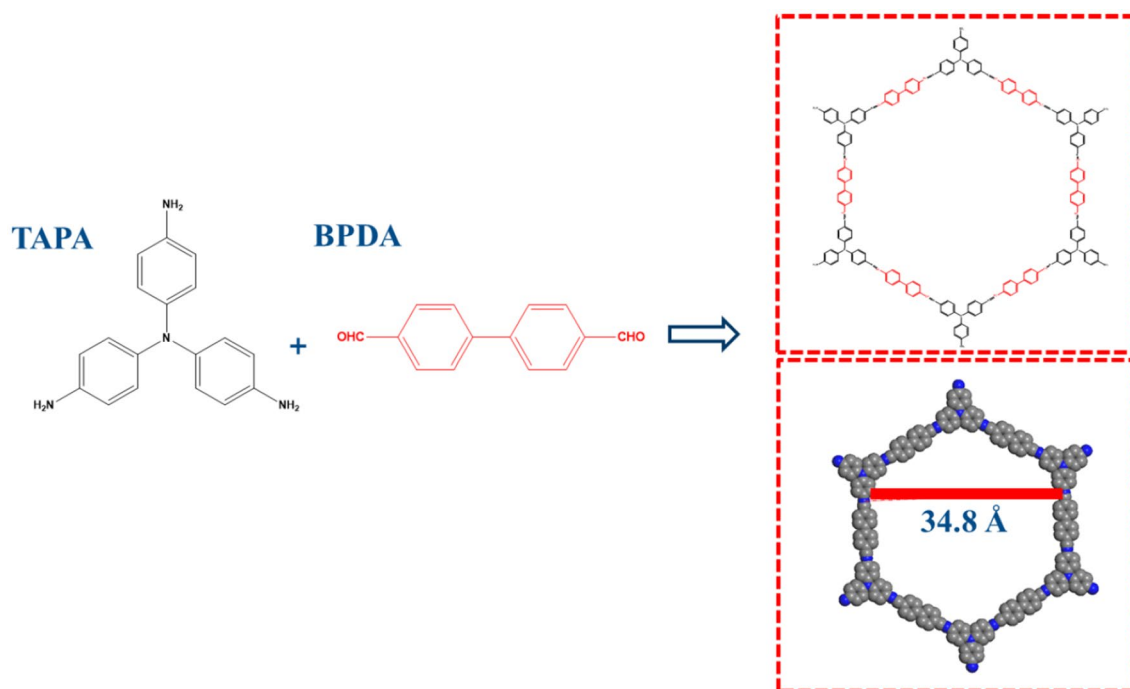


**Fig. 2** Schematic diagram of the synthetic process and molecular structure of TABP-COF.

## Results and Discussion

### Morphology and Structure of TABP-COF

In order to explore the growth process of TABP-COF, the SEM images of TABP-COF materials with different reaction times were observed (Fig. 3). In the SEM images, we found that the morphology of TABP-COF changed continuously as the reaction time increased. TABP-COF showed a staggered arrangement of nanosheets (Fig. 3a) when the reaction time was 24 h, which is attributed to the formation of microcrystalline polymers. When the reaction time was increased to 48 h, the staggered arrangement of nanosheets gradually transformed to spheroid, but some nanosheets could be found around the spheroid (Fig. 3b). Finally, an entire spherical COF was obtained when the reaction time was 72 h (Fig. 3c). The reason for the self-assembly of TABP-COF into a spherical morphology by microcrystalline nanosheet array is that the growth process of the COF material is a slow and reversible crystallization process.[29] Compared with COF nanosheet, the spherical COF structure is more stable and regular, which improves the stability and crystallinity of the material.

Figure 4a shows the FTIR spectra of two monomers. The peaks at 3408 cm$^{-1}$ and 3333 cm$^{-1}$ represent N–H bending vibration, and the peak at 1697 cm$^{-1}$ represents C=O stretching vibration, which correspond to the characteristics of the amino and aldehyde groups in the monomer. As can be seen from Fig. 4b, the peak intensity of N–H and C=O vibrations weaken, and C=N stretching vibrations are found at 1619 cm$^{-1}$ as the reaction progresses. The peak at 1494 cm$^{-1}$ corresponds to the substitution of the benzene ring. With the increase in reaction time, the characteristic peaks of N–H and C=O gradually decrease, and the characteristic peak of C=N gradually increases, indicating that the reversible reaction proceeds in the forward direction with the increase in reaction time.[30] Thus, TABP-COF was synthesized successfully when the reaction time was 72 h.

Figure 5 exhibits the Raman spectra of TAPA, BPDA, and the TABP-COF materials at different reaction times. The characteristic peaks of TAPA (1354 cm$^{-1}$, $v$ –NH$_2$)
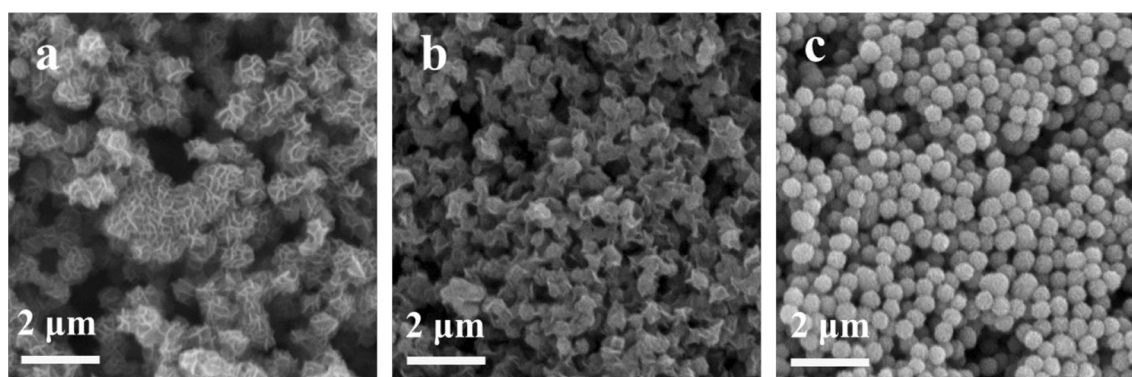


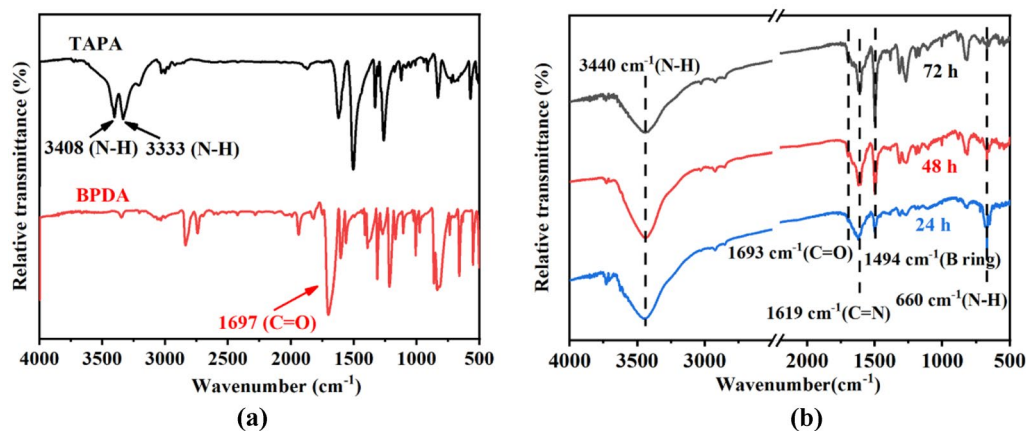**Fig. 3** SEM images of TABP-COF-1 (a), TABP-COF-2 (b) and TABP-COF-3 (c).



**Fig. 4** FTIR spectra of TAPA, BPDA (a), and TABP-COF at different reaction times (b).

and BPDA (1696 cm$^{-1}$, ν C=O) building units disappear in TABP-COF as the reaction time increases. TABP-COFs prepared with different times exhibit similar Raman spectra. The peak of 1595 cm$^{-1}$ represents C=C vibration in benzene units. The peak of 1651 cm$^{-1}$ represents the C=N band, which gradually increases with increasing reaction time. The Raman spectra also confirm the successful synthesis of TABP-COF when the reaction time is 72 h, further confirming the results of the FTIR spectra.

The crystal structure of the COF influences its stability.[31,32] To further investigate the crystal structure of the samples, x-ray diffraction (XRD) tests of the TABP-COF materials were carried out with different reaction times, as shown in Fig. 6a. TABP-COF-1 and TABP-COF-2 mainly exhibit an amorphous structure with a low degree of
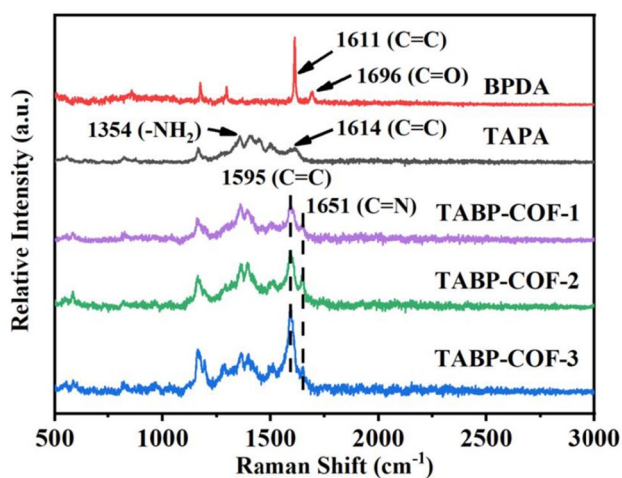


**Fig. 5** Raman spectra of TAPA, BPDA, and TABP-COF at different reaction times.

crystallinity. TABP-COF-3 shows the typical (100) crystal plane at 5.8°, and the (110), (210), and (001) crystal faces at 8.8°, 13.6°, and 23.9°, respectively. In particular, the peak strength of the (001) crystal face of TABP-COF-3 is high, which corresponds to the interlayer π–π accumulation of COF material as shown in Fig. 6b.[33]

Figure 7 shows the TGA curves of TABP-COF at different reaction times. All curves of TABP-COF exhibit a similar mass reduction trend. As shown in Fig. 7, the first stage of thermogravimetric loss before 200°C is mainly due to the evaporation of residual solvent remaining in the nanopores of samples. The thermogravimetric loss between 450°C and 500°C is due to decomposition of nanocrystalline powders. When heated to 500°C, the skeleton of the TABP-COF began to collapse, and the covalent bonds broke and carbonized. The weight retention percentages of the samples were calculated as indicated in Fig. 7. It can be seen that the weight retention percentages of TABP-COF-1, TABP-COF-2, and TABP-COF-3 are 33.5%, 49.3%, and 53.7%, respectively. This is because TABP-COF-3 has a more regular molecular configuration and higher crystallinity, which further confirms the results of the XRD tests.

## Electrochemical and Electrochromic Properties of TABP-COF Electrochromic Films

As shown in Fig. 8, the CV curve of the TABP-COF-3 film was tested in a voltage range between −1.5 V and +1.5 V at a scanning rate of 100 mV/s. The obvious redox peaks can be attributed to redox reaction of TPA.[34] The reversible redox reaction of the TABP-COF-3 film proceeded with the change of voltage, and the skeleton of TABP-COF-3 remained stable during the injection and extraction of Li$^+$ in the test system, indicating that TABP-COF-3 has good
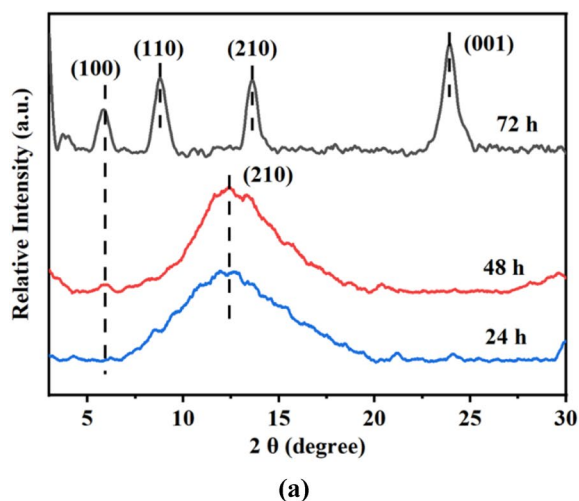


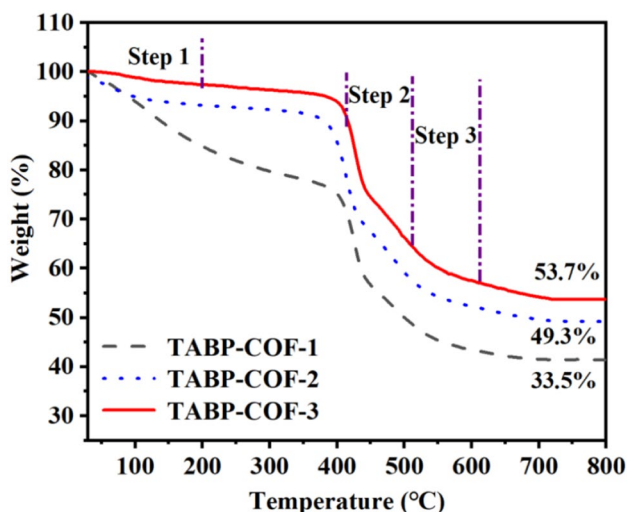**Fig. 6** XRD patterns (a) and molecular structure model (b) of TABP-COF.

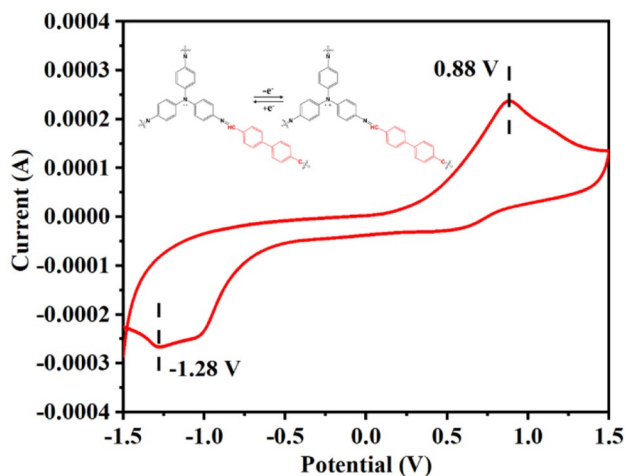**Fig. 7** TGA curves of TABP-COF-1, TABP-COF-2 and TABP-COF-3.



**Fig. 8** CV curves of TABP-COF-3 film (inset is the redox reaction of the COF unit).

electrochemical redox characteristics. The large distance between redox peaks indicates weak reversibility and low conductivity of TABP-COF films. This can be solved by changing the skeleton structure of the COF or by combining COF with high-conductivity materials.

The eigenstates of electrochromic films are determined by their chemical structure. Films undergo reversible redox reactions under different voltages, further changing their band gap and optical properties.[35] In order to determine the electrochromic characteristics of TABP-COF, UV–Vis spectra of TABP-COF-1, TABP-COF-2, and TABP-COF-3 were tested under different voltages, as shown in Fig. 9. Both the eigenstates and bleached state of TABP-COF exhibit yellow films under 0 V and −3.0 V, respectively. The peaks of

eigenstates and bleaching state at 440 nm are attributed to the π–π* electron transfer effect.[27] Electrolyte ions cannot be completely extracted during the electrochemical reaction, and so the spectral curves of eigenstates and bleaching state of TABP-COF films are not completely coincident. When the voltage increases to 1.8 V, a new peak appears at 560 nm, which is due to the appearance of the characteristic absorption peak of polaron-π*.[36] At the same time, the color of the film changes from yellow to brown as shown in Fig. 9c. According to our calculation, the contrast values of TABP-COF-1, TABP-COF-2, and TABP-COF-3 are 0.177, 0.370, and 0.472, respectively, as shown in Table I. Because the crystal orientation of the formed film becomes higher with increasing time, the regular crystal structure promotes charge transfer efficiency and carrier mobility, and then the contrast of TABP-COF-3 film increases.[37] The memory effect is often used to judge the energy-saving efficiency of electrochromic materials by calculating the time at which the film's absorbance decreases to half the absorbance of the colored state after the voltage is removed in the colored state.[38] As shown in Fig. 9d, the memory time of TABP-COF-3 is 308 s, which is related to the stable skeleton structure of TABP-COF-3.

As shown in Fig. 10, the kinetic curves and response times of the TABP-COF-1, TABP-COF-2, and TABP-COF-3 films were tested under step voltages between −3.0 V and +1.8 V, with intervals of 20 s. All curves showed reversible electrochromic behavior under the step voltages. Among them, the contrast of TABP-COF-1 and TABP-COF-2 films decreased rapidly under the swing voltage, which is due to the poor stability of the low crystallinity structure. The irreversible redox process of amorphous films may also be caused by the dimerization of free radical cations in the unstable skeleton structure. In addition, the TABP-COF-3 film retains the initial contrast under alternating voltages, which corresponds to the results of structural characterization of TABP-COF-3. The coloring time ($t_c$), defined as the time it takes for the film's contrast to achieve 90% of its maximum contrast, is a crucial factor in evaluating electrochromic performance.[39] Similarly, the bleaching time ($t_b$) is defined as the time required for 10% ΔA.[40] As listed in Table I, the response time decreases as the reaction time increases, which further demonstrates that the reaction process of TABP-COF-3 is thorough. Due to the higher regularity of the AA stack, TABP-COF-3 not only transfers electrons in-plane, but also provides ion movement paths in the direction of the vertical plane.

In order to investigate the resistance of TABP-COF at different reaction times, electrochemical impedance spectroscopy of TABP-COF films was measured in a frequency range of $10^{-2}$–$10^{5}$ Hz (Fig. 11). The impedance curves of TABP-COF films do not show obvious semi-arc in the high frequency region, which is due to the contact resistance
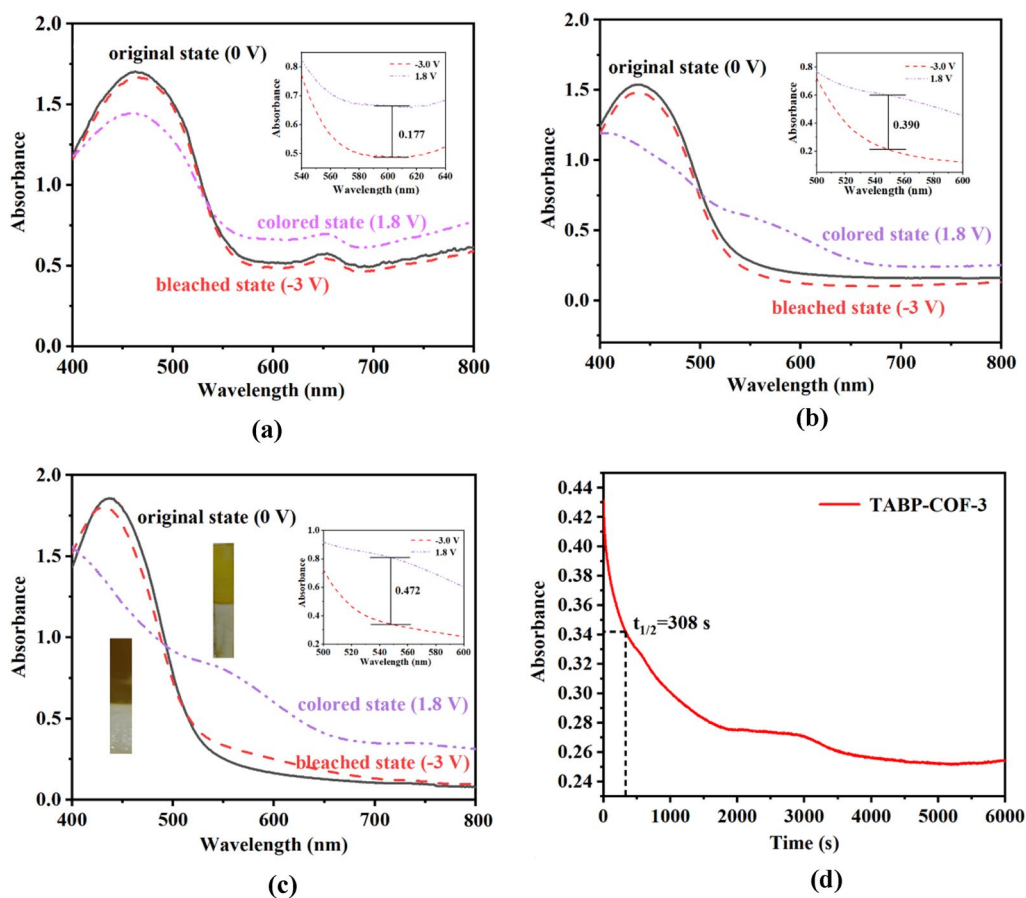
**Fig. 9** UV–Vis spectra of TABP-COF-1 film (a), TABP-COF-2 film (b), and TABP-COF-3 film (c) in original state, colored state, and bleached state, respectively, and memory effect test of TABP-COF-3 (d) (insets are a magnification of the wavelength at 500–600 nm) (Color figure online).

**Table 1** Contrast and response time of TABP-COF at different reaction time

| Sample | Contrast | $t_c$ (s) | $t_b$ (s) |
| --- | --- | --- | --- |
| TABP-COF-1 | 0.177 | 14.2 | 16.7 |
| TABP-COF-2 | 0.370 | 12.0 | 17.1 |
| TABP-COF-3 | 0.472 | 7.3 | 13.6 |

between the film and the electrolyte, and the resistance of the electrolyte itself, are too large.[41] In the mid-frequency region and the low-frequency region, the impedance curve of TABP-COF-3 film is closer to the vertical axis because of the lower diffusion resistance of TABP-COF-3. We used the ZimDemo software to fit the impedance data and obtained the circuit diagram as shown in the inset of Fig. 11. The impedance of TABP-COF films mainly includes the contact resistance ($R_s$), charge transfer resistance ($R_{ct}$) and Warburg resistance ($Z_w$). The $R_s$ values of TABP-COF-1,

TABP-COF-2, and TABP-COF-3 are 387 Ω, 211 Ω, and 150 Ω, respectively. The $R_{ct}$ values of TABP-COF-1, TABP-COF-2, and TABP-COF-3 are 121 Ω, 86 Ω, and 53 Ω, respectively. The $Z_w$ values of TABP-COF-1, TABP-COF-2, and TABP-COF-3 are 33 Ω, 25 Ω, and 19 Ω, respectively. TABP-COF-3 has the smallest resistance and highest charge transfer efficiency, which corroborates previous results and confirms that TABP-COF-3 film is the most suitable for fabricating electrochromic material.

## Conclusion

We have successfully synthesized TABP-COF electrochromic material based on a TPA unit by a solvothermal method. The influence of the TABP-COF reaction time on the structure and electrochromic performance was investigated. The growth of the TABP-COF proceeded in a self-assembly process from a nanosheet array to a spherical shape. The crystallinity of the TABP-COF increased with
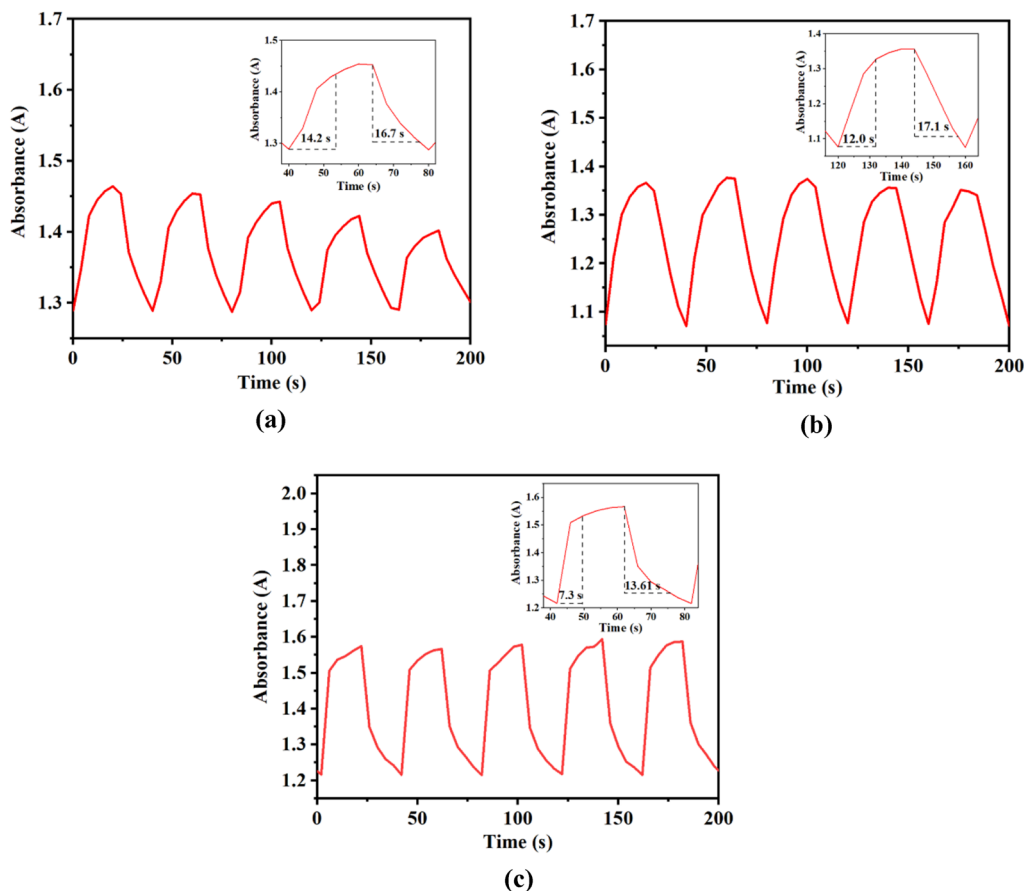
**Fig. 10** Kinetic test and response time test of TABP-COF-1 film (a), TABP-COF-2 film (b), and TABP-COF-3 film (c) (insets are magnifications of memory time).
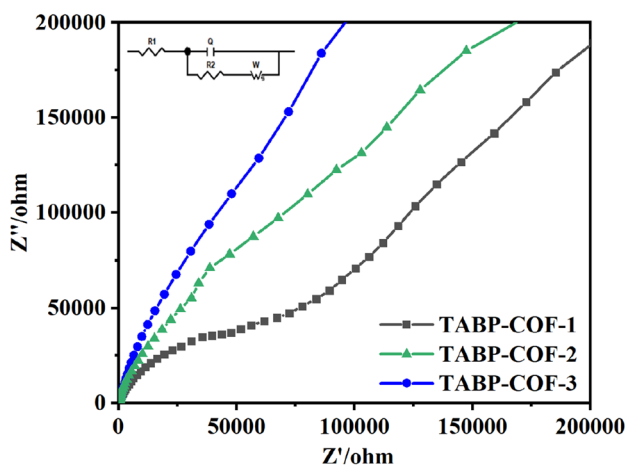


**Fig. 11** Nyquist plots of TABP-COF films at different reaction times (inset is the equivalent circuit).

a homogeneous yellow film on the surface of ITO conductive glass. In electrochemical tests, the EIS test showed that the conductivity of TABP-COF-3 film was enhanced. The CV curve showed that the TPA active unit provides reversible redox properties for the films. The results of UV–Vis spectroscopy showed that the film thickness and the optical contrast of the TABP-COF-3 film increased. TABP-COF-3 film also exhibited a reversible color change from yellow to brown at voltages of −3.0 V and +1.8 V, and the response times of TABP-COF-3 film were 7.3 s/13.6 s. The application of COF in the area of electrochromic materials has excellent potential due to the tunability of its structure. The potential applications of these findings are mainly focused on the production of multifunctional electrochromic devices and the development of smart windows.

the increase in reaction time. A more regular arrangement of molecules provides pathways for interlayer transport of ions. When the reaction time was 72 h, TABP-COF-3 exhibited

# References

1. H.X. Guo, Y. Zhang, S. Wang, L. Li, W. Wang, and Q. Sun, In-situ generation of $Bi_2S_3$ to construct $WO_3/BiVO_4/Bi_2S_3$ heterojunction for photocathodic protection of 304SS. *J. Electroanal. Chem.* 907, 116033 (2022).

2. J.R. Platt, Electrochromism, a possible change of color producible in dyes by an electric field. *J. Chem. Phys.* 34, 862 (1961).

3. M. Rozman, L. Bostjanmatoh, F. Regina, S. Argyroula, and E. Urbanluksic, Flexible electrochromic tape using steel foil with $WO_3$ thin film. *Electrochim. Acta* 330, 135329 (2020).

4. W.E. Donath, J.C. Powers, W.R. Heller, and J. Kumamoto, Stark effect of phenol blue (electrochromism). *J. Am. Chem. Soc.* 86, 1004 (1964).

5. E. Hopmann, A.Y. Elezzabi, W. Zhang, and H. Li, Nanostructured inorganic electrochromic materials for light applications. *Nanophotonics* 10, 825 (2020).

6. D. Ma, and J. Wang, Inorganic electrochromic materials based on tungsten oxide and nickel oxide nanostructures. *Sci. China: Chem.* 60, 54 (2017).

7. B.J. Holliday, Y. Liang, D. Strohecker, V. Lynch, and R.A. Jones, A thiophene-containing conductive metallopolymer using an Fe(II) Bis(terpyridine) core for electrochromic materials. *ACS Appl. Mater. Interfaces* 8, 34568 (2016).

8. F. Li, T.-C. Yen, and G.-S. Liou, Synthesis of high-performance electrochromic material for facile fabrication of truly black electrochromic devices. *Electrochim. Acta* 367, 137474 (2021).

9. N. Huang, L.P. Zhai, D.E. Coupry, M.A. Addicoat, K. Okushita, K. Nishimura, T. Heine, and D.L. Jiang, Multiple-component covalent organic frameworks. *Nat. Commun.* 7, 12325 (2016).

10. S. Ding, W. Wang, S. Ding, and W. Wang, Covalent organic frameworks (COFs): from design to applications. *Chem. Soc. Rev.* 42, 548 (2013).

11. C.J. Kang, Z.Q. Zhang, A.K. Usadi, D.C. Calabro, L.S. Baugh, K.X. Yu, Y.X. Wang, and D. Zhao, Aggregated structures of two-dimensional covalent organic frameworks. *J. Am. Chem. Soc.* 7, 144 (2022).

12. Y.H. Zhu, S.Y. Jiang, X.C. Jing, and X. Feng, Electrically conductive 2D covalent organic frameworks. *Trends Chem.* 4, 128 (2021).

13. L. Jianguo, W. Nan, and Ma. Longlong, Recent advances in covalent organic frameworks for catalysis. *Chem.-Asian J.* 15, 338 (2020).

14. W.-K. Qin, C.-H. Tung, and L.-Z. Wu, Covalent organic framework and hydrogen-bonded organic framework for solar-driven photocatalysis. *J. Mater. Chem. A* 11, 12521 (2023).

15. S. Das, J. Feng, and W. Wang, Covalent organic frameworks in separation. *Annu. Rev. Chem. Biomol. Eng.* 11, 112019 (2020).

16. R. Iqbal, An electrochemically stable 2D covalent organic framework for high-performance organic supercapacitors. *Chin. J. Polym. Sci.* 38, 8 (2020).

17. C.J. Yao, Z.Z. Wu, J. Xie, F. Yu, W. Guo, Z.C.J. Xu, S.Q. Zhang, and Q.C. Zhang, Two-dimensional (2D) covalent organic framework as efficient cathode for binder-free lithium-ion battery. *Chemsuschem* 13, 2457 (2020).

18. M.S. Lohse, and T. Bein, Covalent organic frameworks: structures, synthesis, and applications. *Adv. Funct. Mater.* 28, 1705553 (2018).

19. L. Liu, D. Cui, S.R. Zhang, W. Xie, C. Yao, and Y.H. Xu, Integrated carbon nanotube and triazine-based covalent organic framework composites for high capacitance performance. *Dalton Trans.* 52, 2762 (2023).

20. S.X. Xiong, Y.K. Zhang, J.J. Zhang, X.Q. Wang, J. Chu, R.L. Zhang, M. Gong, B.H. Wu, and G.Q. Liu, Solvothermal synthesis and enhanced electrochromic properties of covalent organic framework/functionalized carbon nanotubes composites electrochromic materials with anthraquinonoid active unit. *Sol. Energy Mater. Sol. Cells* 235, 111489 (2022).

21. S.X. Xiong, Y.C. Wang, X.Q. Wang, J. Chu, R.L. Zhang, M. Gong, B.H. Wu, and Z. Li, Schiff base type conjugated organic framework nanofibers: solvothermal synthesis and electrochromic properties. *Sol. Energy Mater. Sol. Cells* 209, 110438 (2021).

22. Q. Hao, Z.J. Li, C. Lu, B. Sun, Y.W. Zhong, L.J. Wan, and D. Wang, Oriented two-dimensional covalent organic framework films for near-infrared electrochromic application. *J. Am. Chem. Soc.* 141, 19831 (2019).

23. Q. Hao, B. Zhi-Juanbai, Y.-W. Xingzhong, and D. Li-Junwang, A covalent organic framework film for three-state near-infrared electrochromism and a molecular logic gate. *Angewandte Chemie* 60, 12498 (2021).

24. R. Zheng, J. Zhang, C. Jia, Z. Wan, Y. Fan, X. Weng, J. Xie, and L. Deng, A novel self-healing electrochromic film based on a triphenylamine cross-linked polymer. *Polym. Chem.* 8, 6981 (2017).

25. R.Z. Zheng, J.Q. Zhang, C.Y. Jia, Z.Q. Wan, Y.R. Fan, X.L. Weng, J.L. Xie, and L.J. Deng, Synthesis and characterization of stable electrochromic polyimides with quinolin-8-yloxy-substituted triphenylamine units. *J. Electroanal. Chem.* 801, 388 (2017).

26. Y. Yan, N.W. Sun, X.T. Jia, X.C. Liu, C. Wang, and D.M. Chao, Electrochromic and electrofluorochromic behavior of novel polyurea bearing oligoaniline and triphenylamine units. *Polymer* 134, 1 (2018).

27. S. Cai, S. Wang, D. Wei, H. Niu, W. Wang, and B. Xuduo, Multifunctional polyamides containing pyrrole unit with different triarylamine units owning electrochromic, electrofluorochromic and photoelectron conversion properties. *J. Electroanal. Chem.* 812, 132 (2018).

28. L. Cao, I.C. Chen, X.W. Liu, Z. Li, Z.Y. Zhou, and Z.P. Lai, An ionic diode covalent organic framework membrane for efficient osmotic energy conversion. *ACS Nano* 16, 18910 (2022).

29. H. Chen, X. Yuan, H. Wang, Yu. Hanbo, and L. Jiang, Nanostructured covalent organic frameworks with elevated crystallization for (electro)photocatalysis and energy storage devices. *J. Mater. Sci.* 56, 13875 (2021).

30. S.B. Raoni, R.S. Gonçalves, A.B. de Oliveira, H.C. Sindra, B.S. Archanjo, M.E. Mendoza, L.S. Carneiro, C.D. Buarque, and P. Esteves, Heterogeneous catalysis by covalent organic frameworks (COF): Pd(OAc)2@COF-300 in cross-coupling reactions. *Chemcatchem* 8, 743 (2016).

31. D.L. Ma, C. Qian, Q.Y. Qi, Z.R. Zhong, G.F. Jiang, and X. Zhao, Effects of connecting sequences of building blocks on reticular synthesis of covalent organic frameworks. *Nano Res.* 14, 381 (2020).

32. F. Lv, S. Xiong, J. Zhang, X. Wang, J. Chu, R. Zhang, M. Gong, B. Wu, G. Liu, and W. Luo, Enhanced electrochromic properties of 2,6-diaminoanthraquinone and 1,3,5-triformylresorcinol (DAAQ-TFP) covalent organic framework/functionalized graphene oxide composites containing anthraquinone active unit. *Electrochim. Acta* 398, 139301 (2021).

33. X. Liu, Y. Wang, Y. Liu, L.I. Zonglong, L.I. Hui, Q. Fang, and Y. Jin, A covalent organic framework with high surface area for drug delivery. *Chem. Res. Chin. Univ.* 40, 1813 (2019).

34. Y. Ji, H.J. Niu, H.Y. Zhang, W.J. Wu, J.W. Cai, C. Wang, X.D. Bai, and W. Wang, Synthesis and electrochromic properties of

polybismaleimides containing triphenylamine units. *J. Solid State Electrochem.* 18, 1537 (2014).

35. R. Brooke, J. Edberg, D. Iandolo, M. Berggren, X. Crispin, and I. Engquist, Controlling the electrochromic properties of conductive polymers using UV-light. *J. Mater. Chem. C.* 6, 4663 (2018).

36. N.B. Teran, and J.R. Reynolds, Discrete donor-acceptor conjugated systems in neutral and oxidized states: implications toward molecular design for high contrast electrochromics. *Chem. Mater.* 29, 1290 (2017).

37. X.Y. Yang, L. Gong, K. Wang, S.H. Ma, W.P. Liu, B.W. Li, N. Li, H.H. Pan, X. Chen, H.L. Wang, J.M. Liu, and J.Z. Jiang, Ionothermal synthesis of fully conjugated covalent organic frameworks for high-capacity and ultrastable potassium-ion batteries. *Adv. Mater.* 34, e2207245 (2022).

38. G. Balamurugan, and J.S. Park, Metallo-terpyridine modified asymmetric viologen exhibiting remarkable optical memory effect in single-layered electrochromic devices. *Electrochim. Acta* 382, 138308 (2021).

39. C.-P. Constantin, and M.-D. Damaceanu, A refreshing perspective on electrochromic materials: phenoxazine as an opportune moiety towards stable and efficient electrochromic polyimides. *Chem. Eng. J.* 465, 142883 (2023).

40. W. Liu, X. Zhang, J. Liu, X. Ma, J. Zeng, P. Liu, and T. Xu, Electrochromic properties of organic-inorganic composite materials. *J. Alloys Compd.* 718, 379 (2017).

41. A.A. Moya, Electrochemical impedance of ion-exchange membranes with interfacial charge transfer resistances. *J. Phys. Chem. C* 120, 6543 (2016).